BIOENGINEERING

Amphiphilic and fatigue-resistant organohydrogels for small-diameter vascular grafts

Jinfei Hou[1]†, Xu Zhang[2,3,4]†, Yuqiong Wu[5], Junjin Jie[1], Zhenxing Wang[1], Guo-Qiang Chen[2,3,4]*, Jiaming Sun[1]*, Lin-Ping Wu[5]*

Hydrogels are used in vascular tissue engineering because of their good biocompatibility. However, most natural hydrogels exhibit high swelling ratio, poor mechanical stability, and low durability, which are key limitations for wider applications. Amphiphilic and fatigue-resistant organohydrogels were fabricated here via the click chemical reaction of unsaturated functional microbial polyhydroxyalkanoates and polyethylene glycol diacrylate and a combination of two-dimensional material graphdiyne. These organohydrogels were maintained stable in body fluids over time, and their tensile moduli remained unchanged after more than 2000 cycles of cyclic stretching. The tubular scaffolds presented good biocompatibility and perfusion in vitro. After transplantation in vivo, the vascular grafts exhibited obvious cell infiltration and tissue regeneration, having a higher patency rate than the control group in 3 months. This fabrication method provides a strategy of improving and promoting the application of organohydrogels as implant materials for small-diameter vascular graft.

INTRODUCTION

Hydrogels with remarkable characteristics, including tunable physical, chemical, and biological properties; excellent biocompatibility; and similarity to the native extracellular matrix (ECM) have widespread applications in biomedicine, including in regenerative medicine (*1*, *2*), drug delivery (*3*), stem cell therapy (*4*), and cancer research (*5*). Regarding blood vessel repair, hydrogels have the advantages of mass transport and promotion of vascular network formation, which makes them promising materials for vascular grafts (*6*–*8*). However, the inherent swelling properties severely decrease the mechanical performance, which may result in instability and deformation of the hydrogel (*9*). Thus, it is essential to prepare nonswelling hydrogels under body fluid conditions, especially for vascular tissue repair. Furthermore, most biocompatible hydrogels exhibit poor mechanical behavior and are prone to fatigue with cyclic stretching (*2*). Hence, they obviously do not conform to the standards of vascular prostheses, which must withstand up to 400 to 600 million loading cycles according to the U.S. Federal Regulatory Authority (*10*).

To achieve the application of hydrogels with small-diameter (2- to 6-mm) vascular grafts (SDVGs), methods such as applying centrifugal forces, incorporating porous meshes, and fabricating double-network hydrogels have been used to enhance the mechanical properties and stabilities of SDVGs (*11*). Although these methods have been successful, their transition to clinical use has been hampered by numerous technological obstacles. Initially, it is necessary for hydrogels to have antiswelling properties to enable their long-term stability in the body (*9*, *12*). Second, hydrogels must have fatigue-resistant and mechanical properties matching those of vascular tissues (*13*). Third, effective diffusion and perfusion are essential for vascular grafts to transport oxygen, nutrients, and waste products and to promote cellular infiltration, which is related to the surface structure of the hydrogel (*11*). Last, to facilitate the translation of synthetic hydrogel vascular grafts from bench to bedside, these scaffolds must maintain high patency rates after implantation for a long time (*10*, *11*, *14*).

To overcome these technical barriers, we propose organohydrogels with flexible amphiphilicity, enhanced mechanical properties, and fatigue resistance. The fabrication process relies on the click chemistry reaction of unsaturated functional polyhydroxyalkanoates (PHAs) and polyethylene glycol diacrylate (PEGDA) and a mixture of uniformly dispersed graphdiyne (GDY) nanoparticles. Organohydrogels, inspired by the concept of "binary cooperative complementary," have emerged as promising "nonswelling" hydrogels with specific properties (*15*–*18*). In addition to their basic amphipathicity, organohydrogels have various properties such as freeze tolerance (*17*), shape memory (*19*), and reconfigurable surfaces (*20*). Thus, organohydrogels have been widely applied in soft robotics, flexible electronics, and bioinspired ionic skin.

However, very few scholars have explored organohydrogels as implanted biomaterials, because the organic components of most organohydrogels previously reported were not suitable for use in vivo or even toxic to creatures, such as lauryl methacrylate and *n*-butyl methacrylate. Although the amphipathicity of the organohydrogels obviously contributed to the stability of the gels, the biocompatibility of organohydrogels remains a challenge, hindering their further application in vivo. Here, PHA is a family of biopolyesters accumulated by various bacteria and is widely used in medical applications because of their excellent biodegradability and biocompatibility with favorable thermal and mechanical properties (*21*, *22*). According to the related research, it can be inferred that PHA is a potential and appropriate organic component for fabrication of biocompatible organohydrogels (*23*, *24*). In addition, previous scholars have made efforts to engineer high-mechanical hydrogels through the incorporation of nanomaterials such as carbon

[1]Department of Plastic Surgery, Union Hospital, Tongji Medical College, Huazhong University of Science and Technology, Wuhan 430022, China. [2]Department of Chemical Engineering, Tsinghua University, Beijing 100084, China. [3]Key Laboratory of Industrial Biocatalysis, Ministry of Education, Tsinghua University, Beijing 100084, China. [4]Center of Synthetic and Systems Biology, School of Life Sciences, Tsinghua-Peking Center for Life Sciences, Tsinghua University, Beijing 100084, China. [5]Center for Chemical Biology and Drug Discovery, Guangzhou Institute of Biomedicine and Health, Chinese Academy of Sciences, Guangzhou 510530, People's Republic of China.
*Corresponding author. Email: chengq@mail.tsinghua.edu.cn (G.-Q.C.); sunjm1592@sina.com (J.S.); wu_linping@gibh.ac.cn (L.-P.W.)
†These authors contributed equally to this work.

nanotubes and graphene oxide with hydrogel networks composed of natural or synthetic liquid polymers (*13*, *25*). However, the newly found two-dimensional (2D) GDY with higher stability and enhancement of cell adhesion has not been reported in this sort of study.

The present study constructed amphiphilic, fatigue-resistant, and biocompatible PHA/PEGDA-GDY organohydrogels forming SDVGs and characterized the swelling rate, surface structure, stability, mechanical properties, fatigue resistance of the organohydrogels, biocompatibility, and functional perfusion of the fabricated vascular scaffold in vitro. The possibility of the PHA component applied as an organic network of biocompatible organohydrogels was tested, and GDY nanoparticles were first used to enhance gel mechanics and tailored the microstructure of biomedical scaffolds. The repair of vascular defects with a PHA/PEGDA-GDY organohydrogel vascular graft was evaluated after being surgically implanted into rodent models. The patency rate, immunological rejection, and tissue regeneration of organohydrogel vascular grafts were measured to evaluate their feasibility as SDVGs for further applications.

RESULTS

Fabrication and characterization of PHA/PEGDA-GDY organohydrogels

Poly(3-hydroxybutyrate-*co*-3-hydroxy-10-undecenoate) (P3HB10U), a type of unsaturated functional PHA, was biosynthesized using the carbon sources glucose and 10-undecenoic acid by engineered *Pseudomonas entomophila*, with its chromosomal β-oxidation pathway weakened and 3-hydroxybutyrate synthesis pathway inserted (*23*), following with characterized by nuclear magnetic resonance (NMR) spectroscopy (fig. S1). Figure 1 illustrates the fabrication procedure of the PHA/PEGDA-GDY organohydrogels. The PHA organogels were important components of the organohydrogels with adjustable degrees of cross-linking during the photocrosslinking reaction (*24*). After assessing the cross-linking time and adhesion of the organogels (fig. S2), the chosen PHA organogels were prepared using microbial polymer P3HB10U with 45% alkene and 2000-Da PEG-dithiol at equivalents of 0.25. The peaks of carbonyl and —CH═CH_2 stretching in the Fourier transform infrared (FTIR) spectrum indicated that P3HB10U and PEGDA were cross-linked via a click reaction (fig. S3). The amphipathicity of organohydrogels was determined by the ratio of the PHA organogel to PEGDA hydrogel. PHA/PEGDA organohydrogels fabricated using PHA organogel and PEGDA hydrogel at a weight ratio of 1:1 showed appropriate hydrophilicity and hydrophobicity (Fig. 2 and fig. S4), and their biocompatibility was similar to those of organohydrogels at the other ratios (fig. S5). In the following experiments, all PHA/PEGDA organohydrogels were fabricated at a weight ratio of 1:1 (PHA organogel:PEGDA hydrogel). The interpenetrating network structure of the organohydrogels spatially limited the hydrophilic/oleophilic networks with respect to each other (*17*). Consequently, the volume of the organohydrogels could remain stable when they were equilibrated in organic or aqueous phase, a notable difference from the volume changes observed in homogeneous networks of organogels or hydrogels. The PHA organogels shrink when equilibrated in water, and the same material remained in a swollen state after being immersed in oil. The PEGDA hydrogels exhibited the opposite phenomena: swelling in water but shrinking in oil (Fig. 2A). The diameters and swelling ratios of the PHA/PEGDA organohydrogels remained constant regardless of whether they were equilibrated in oil or water, as did those of the PHA/PEGDA-GDY organohydrogels (Fig. 2, B and C). The contact angles (CAs) of the PHA/PEGDA and PHA/PEGDA-GDY organohydrogels were 48.8° and 44.1° in the aqueous phase and 28.07° and 31.03° in the organic phase, respectively (fig. S6); these values are within the ranges of those of PHA organogels and PEGDA hydrogels. The amphipathicity of the PHA/PEGDA-GDY organohydrogels was further verified by the surface-free energy (SFE) (fig. S7). In addition, it was confirmed that the dispersion of the GDY nanoparticles did not affect the favorable characteristics of pure PHA/PEGDA organohydrogels such as amphipathicity.

To optimize the concentration of GDY, we used scanning electron microscopy and atomic force microscopy (AFM) to characterize the surfaces of the PHA/PEGDA-GDY organohydrogels with

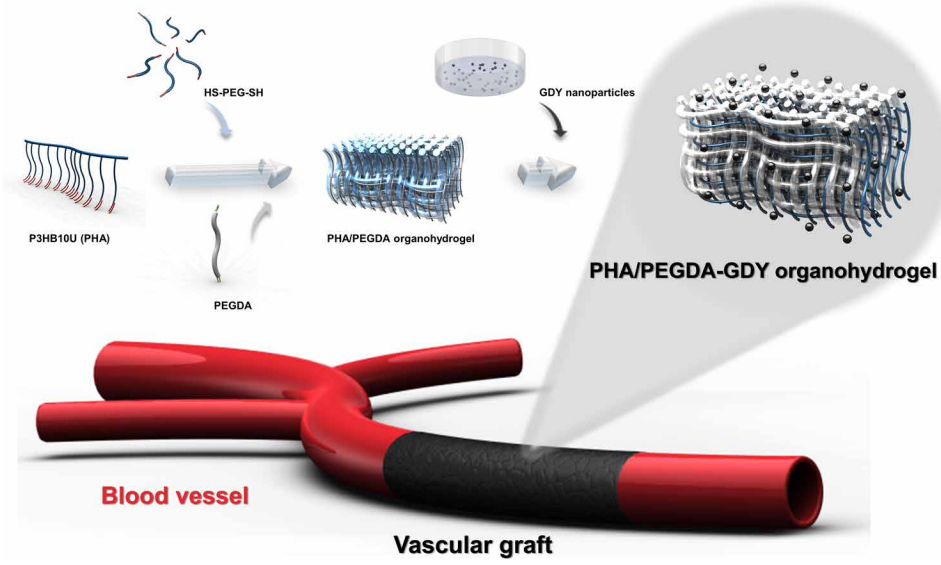

Fig. 1. Illustration of fabrication process for PHA/PEGDA-GDY organohydrogels.

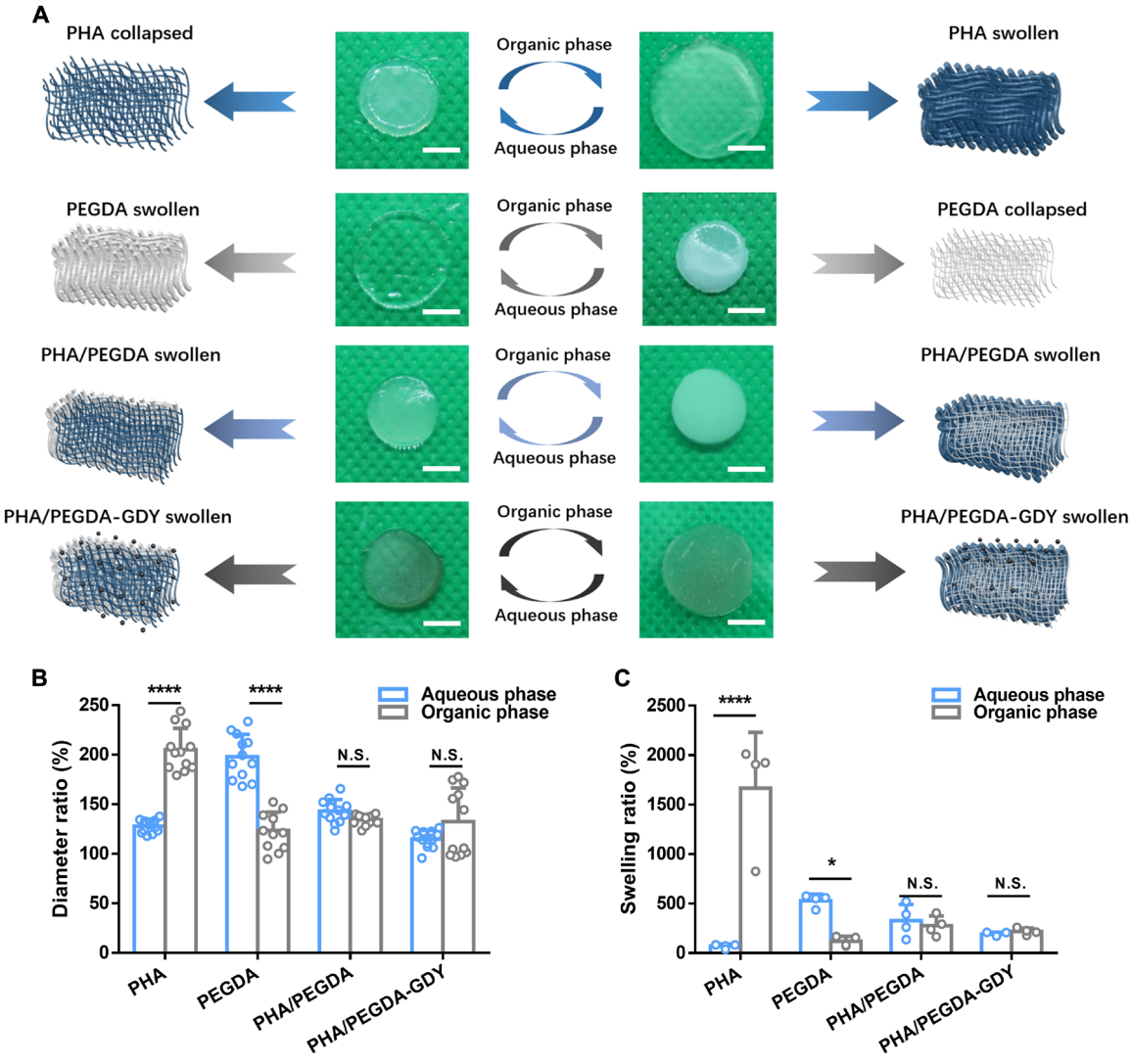

Fig. 2. Swelling performance of different gels. (**A**) Optical images and corresponding schematic of PHA organogels, PEGDA hydrogels, PHA/PEGDA organohydrogels, and PHA/PEGDA-GDY organohydrogels after immersion in aqueous phase and organic phase. Scale bars, 5 mm. (**B**) The diameter ratio and (**C**) swelling ratio of the gels in aqueous phase and organic phase. [$n = 12$ (B) and $n = 4$ (C)]. ****$P < 0.0001$ and *$P < 0.05$ by two-way ANOVA with Sidak correction. N.S., not significant.

different GDY concentrations (Fig. 3 and fig. S8). The GDY nanoparticles exhibited slight aggregation and uneven distribution at a concentration of 0.5%. The effects of GDY at different concentrations on the tensile mechanics and fluid mechanics of PHA/PEGDA-GDY organohydrogels were also investigated (figs. S9 to S11). The PHA/PEGDA-GDY gels with GDY nanoparticle concentrations of 0.1% showed the best mechanical performances, including resistance to shear force and fatigue properties.

The surface structure is important for biomaterials used in tissue engineering. In this study, the organohydrogels were porous (Fig. 3A), and the pore size distributions were analyzed by cryo–electron microscopy (cryo-EM) (Fig. 3, B and C). The pore size of the PHA/PEGDA-GDY organohydrogels was 25.43 ± 7.09 μm, which was much higher than that of the PHA/PEGDA organohydrogels (4.90 ± 1.85 μm). In addition, the GDY nanoparticles were distributed uniformly, and the surface roughness was evaluated using AFM. The PHA/PEGDA-GDY organohydrogels presented the smoothest surfaces among the gels (Fig. 3D), which could be related to the surface stabilization of the GDY nanoparticles.

For most nanoparticle-incorporated gels, the toughness and stiffness of organohydrogels were enhanced through nanoparticle blending. Nevertheless, the presence of these nanoparticles could influence the polymer network and decrease the extensibility by creating weak points and nanoscale defects. The reaction of the PHA organogel and PEGDA hydrogel obviously increased the ultimate strengths and rupture strains of the organohydrogels. The addition of GDY nanoparticles enhanced the tensile moduli of the PHA/PEGDA-GDY organohydrogels but weakened the rupture strain (Fig. 3E and fig. S12). To study the fatigue resistance of the gels, we performed cyclic tensile tests with a maximum strain of 50%. PHA/PEGDA-GDY organohydrogels could endure more than 2000 cycles of loading and unloading, and the tensile modulus remained constant before and after circulation (Fig. 3F and fig. S13A). In the energy loss measurement, the energy loss maintained a low hysteresis contrast to most hydrogels and did not exhibit

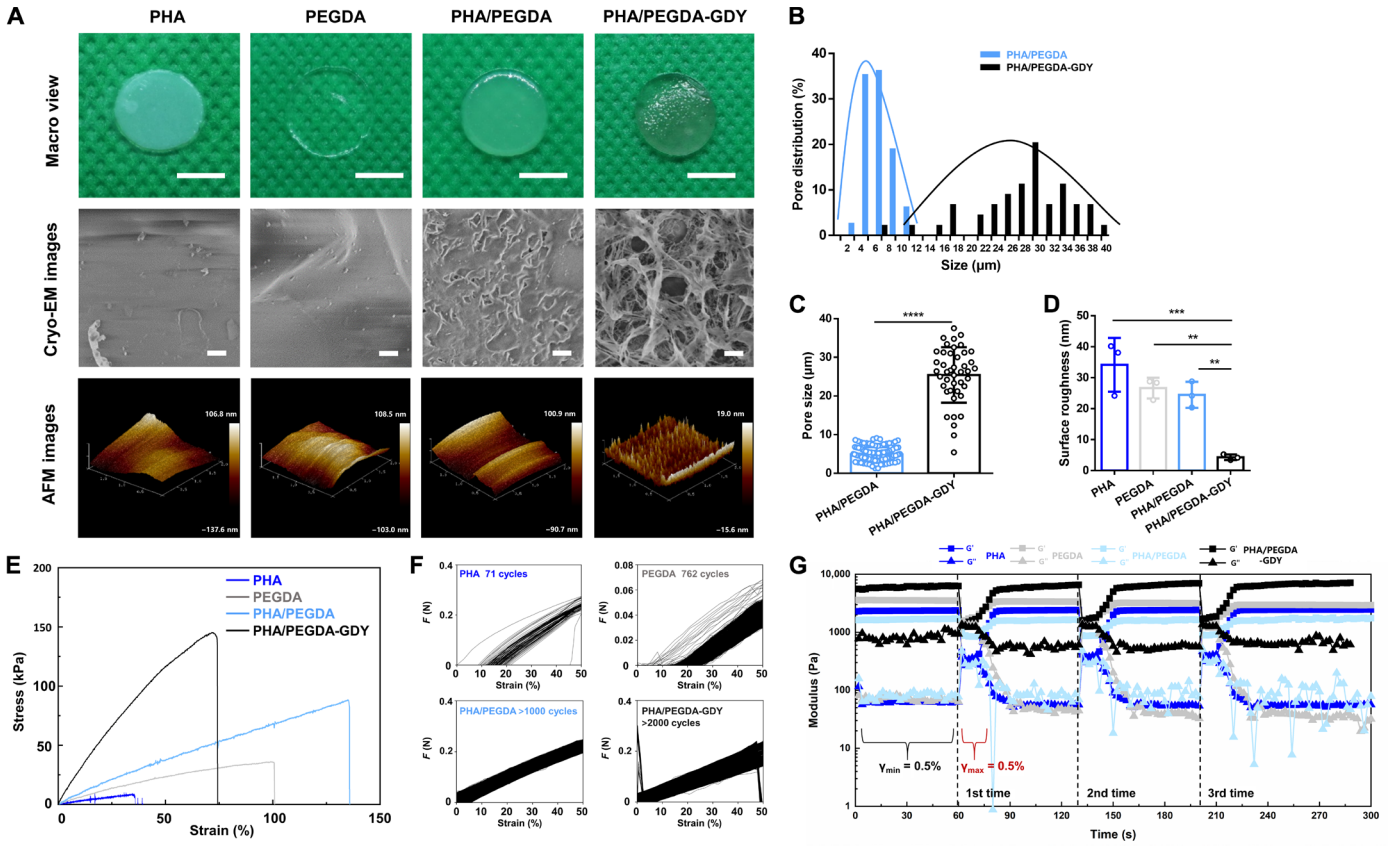

Fig. 3. Surface morphology and mechanical characterizations of different gels. (**A**) Macro view, cryo-EM, and AFM images of the gels. Scale bars, 5 mm (macro view) and 10 μm (cryo-EM images). The concentration of GDY is 0.1%. (**B**) Pore distribution and (**C**) pore size of the organohydrogels have been plotted. ****$P < 0.0001$ by unpaired, two-sided *t* test. (**D**) Surface roughness of the gels was analyzed from AFM images. $n = 3$, ***$P < 0.001$ and **$P < 0.01$ by one-way analysis of variance (ANOVA) with Tukey correction. (**E**) Stress-strain curve under tension of the gels. (**F**) Cyclic tensile test of the gels, demonstrating the maximal number of cycles that gels could bear. (**G**) The modulus as a function of time at a constant frequency of 1 rad/s for the gels at intermittent changes of shear strain amplitudes ($\gamma_{min} = 0.5\%$ and $\gamma_{max} = 100\%$).

deformation after cyclic tests (fig. S13B) (*26*, *27*). The storage moduli of the PHA/PEGDA-GDY organohydrogels exhibited obvious increases (fig. S14, A to C). To test the effects of the short-term shear interval on the viscoelastic properties of the gels, we performed three-interval thixotropic tests (3iTTs) (Fig. 3G). The storage and loss moduli of gels obviously changed after a three-interval shear. The storage moduli of the PHA/PEGDA-GDY organohydrogels slightly increased after three shear intervals compared with those of the other gels (fig. S14D).

Biocompatibility and perfusion of PHA/PEGDA-GDY organohydrogels

The biocompatibility of the gels was evaluated by fluorescein diacetate (FDA)/propidium iodide (PI) staining, immunofluorescence staining of biomarkers, and Cell Counting Kit-8 (CCK8) assay of human umbilical vein endothelial cells (HUVECs) and vascular smooth muscle cells (VSMCs), which are the main cell components of blood vessels. The viability of HUVECs on PHA/PEGDA-GDY organohydrogels was higher than PHA and PHA/PEGDA gels on days 1 and 3 (Fig. 4, A, C, and D; and fig. S15A). Similarly, the viability of VSMCs on PHA/PEGDA-GDY organohydrogels was higher than PHA organogels on days 1 and 3 (Fig. 4, B, E, and F; and fig. S15A).

As is well known, the toxicity of 2D nanomaterials has aroused wide concern and limited their application. Hence, CCK8 assays were used to detect the cell toxicity of the gels. The results indicated that the PHA/PEGDA-GDY organohydrogels had good biocompatibility and safety for HUVECs and VSMCs (fig. S15, B and C). Moreover, the ability of cell adhesion on biomaterials is one of crucial factors for cell proliferation and function. The introduction of GDY nanoparticles into the organohydrogels improved their cell adhesion (fig. S16). HUVECs on PHA/PEGDA-GDY organohydrogels presented well-organized actin filaments, whereas the cells on the other gels showed limited spreading and poorly organized filaments.

To evaluate whether the vascular scaffolds displayed the functional characteristics of blood vessels, we performed perfusion experiments on organohydrogel scaffolds with outer diameters of 3 mm and inner diameters of 2 mm constructed by the molding method. A perfusion device was used and connected to the vascular scaffolds with a plastic pipette inserted into the tube, and the perfusion process was observed under a fluorescent stereoscopic microscope. After injection, it could be clearly observed that the structural integrity of the PEGDA and PHA/PEGDA-GDY scaffolds remained intact, whereas the PHA and PHA/PEGDA scaffolds appeared to fracture in the early seconds, resulting in fluidic leakage (Fig. 5, A and B, and movie S1). The wider diffused distances on the PEGDA scaffolds compared to the PHA/PEGDA-GDY scaffolds were related to the limited water absorption of organohydrogels. Moreover,

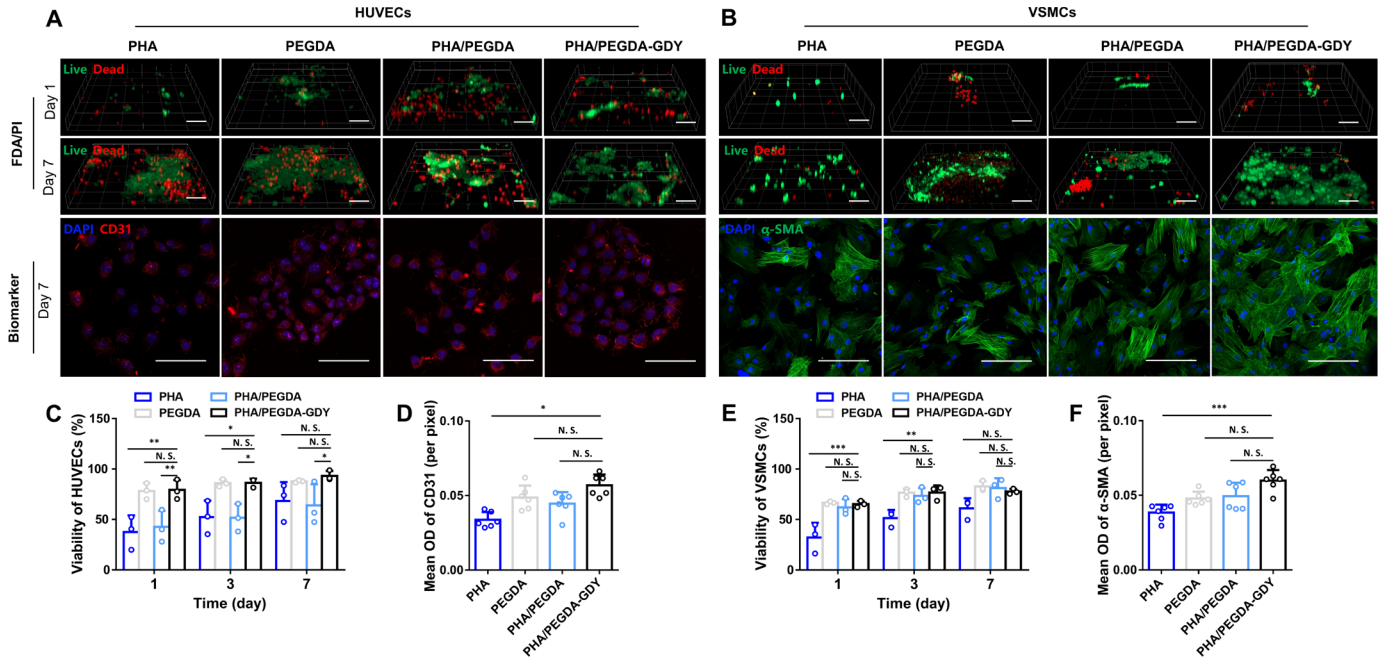

Fig. 4. In vitro cell biocompatibility of different gels. (**A**) HUVECs and (**B**) VSMCs implantation in gels with FDA (green)/PI (red) and corresponding biomarker CD31 (red)/α–smooth muscle actin (α-SMA) (green)/nuclei (blue) immunofluorescence staining. Scale bars, 100 μm (FDA/PI staining) and 200 μm (biomarker staining). Viability of HUVECs (**C**) and VSMCs (**E**) plotted by analysis of the results of biocompatibility experiments. $n = 3$, $^{***}P < 0.001$, $^{**}P < 0.01$, and $^{*}P < 0.05$ by two-way ANOVA with Tukey correction. Mean optical density (OD) of CD31 (**D**) and α-SMA (**F**) were analyzed. $n = 6$, $^{***}P < 0.001$ and $^{*}P < 0.05$ by one-way ANOVA with Sidak correction.

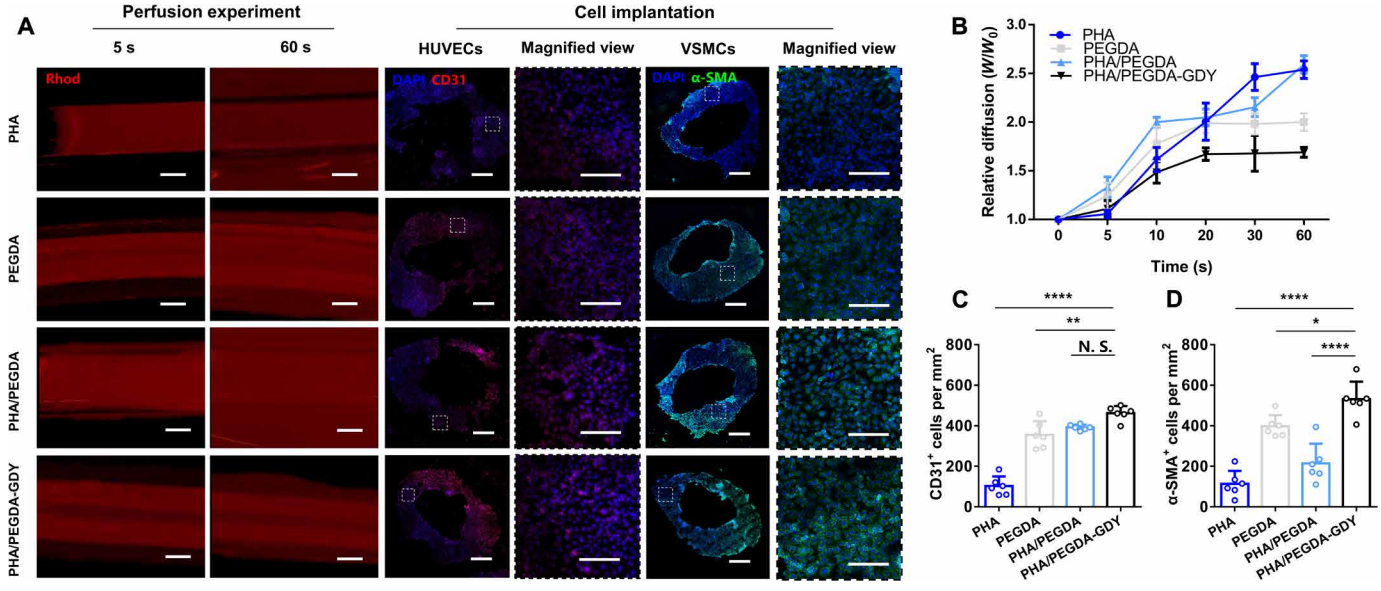

Fig. 5. The perfusion and biological characteristics of gel vascular scaffolds in vitro. (**A**) The perfusion experiment and immunofluorescence staining of cells after implantation in gel vascular scaffolds. Scale bars, 1 mm (perfusion experiment), 500 μm (cell immunofluorescence), and 200 μm (magnified view). (**B**) Relative diffusion of the perfusate through the tube wall (W refer to the width of fluorescent area, and W_0 refers to the original thickness of the vascular scaffolds). (**C**) $CD31^+$ cells and (**D**) $\alpha\text{-SMA}^+$ cells per square millimeter in the slices of scaffolds were calculated from the data analysis of cell implantation. $n = 6$, $^{****}P < 0.0001$, $^{**}P < 0.01$, and $^{*}P < 0.05$ by one-way ANOVA with Tukey correction.

HUVECs and VSMCs were cultured in the vascular scaffolds, and the scaffolds were placed into a homemade bionic perfusion bioreactor to test the vascular functions (fig. S17 and movie S2). There were more cells with positive cellular phenotypes in the PHA/PEGDA-GDY vascular scaffolds (462.33 ± 32.33 HUVECs/mm^2 and 530.67 ± 79.67 VSMCs/mm^2) than on the other groups (Fig. 5, A, C, and D). These results clearly illustrate that the organohydrogels fabricated with GDY provided a better microenvironment for cell proliferation and helped the HUVECs/VSMCs formulate a constant and functionalized vascular tissue–like tubular structure.

In vivo evaluation of the biocompatibility of PHA/PEGDA-GDY organohydrogels in a rat model

To test the basic biocompatibility of the PHA/PEGDA-GDY organohydrogels, we cast gel disks with a thickness of 5 mm and a diameter of 10 mm in a mold and implanted subcutaneously on the dorsa of the rat. Figure 6A demonstrated the timeline of the in vivo biocompatibility experiments. More widespread vascularization could be observed in the PHA/PEGDA-GDY organohydrogels than in the other gels, especially after implantation for 7 days (Fig. 6B and fig. S18). Internal vascularization is important for the biodegradation of scaffolds and tissue regeneration in vivo. With the combination of 0.1% GDY nanoparticles, the PHA/PEGDA-GDY organohydrogels formed a porous microstructure with pores with diameters of approximately 30 μm, which have been proven to promote cell infiltration and related microvascularization (*28*).

To verify the effects of the specific porous structure further, we evaluated cell infiltration of the scaffolds via white-and-black processed hematoxylin and eosin (HE) staining images (Fig. 6C and fig. S19A). The PHA organogels and PEGDA hydrogel disks showed minimal cell infiltration. However, the PHA/PEGDA and PHA/PEGDA-GDY organohydrogels displayed more extensive cell infiltration and tissue regeneration. Quantitative analyses of cell infiltration at different depths throughout the gels were performed on days 3 and 7 (Fig. 6D and fig. S19B). The results indicated that there were more cells in the PHA/PEGDA-GDY organohydrogel scaffold than in the other groups, and the depth of cell penetration in PHA/PEGDA-GDY was the deepest at both 3 and 7 days.

In vivo investigation of PHA/PEGDA-GDY organohydrogel vascular grafts in a rabbit model

In the vascular graft repair experiment, gel vascular grafts were implanted to replace the left carotid arteries of the rabbits. After 1 and 3 months, the samples underwent ultrasonic evaluation and histological detection (Fig. 7A). Because of the poor suture retention

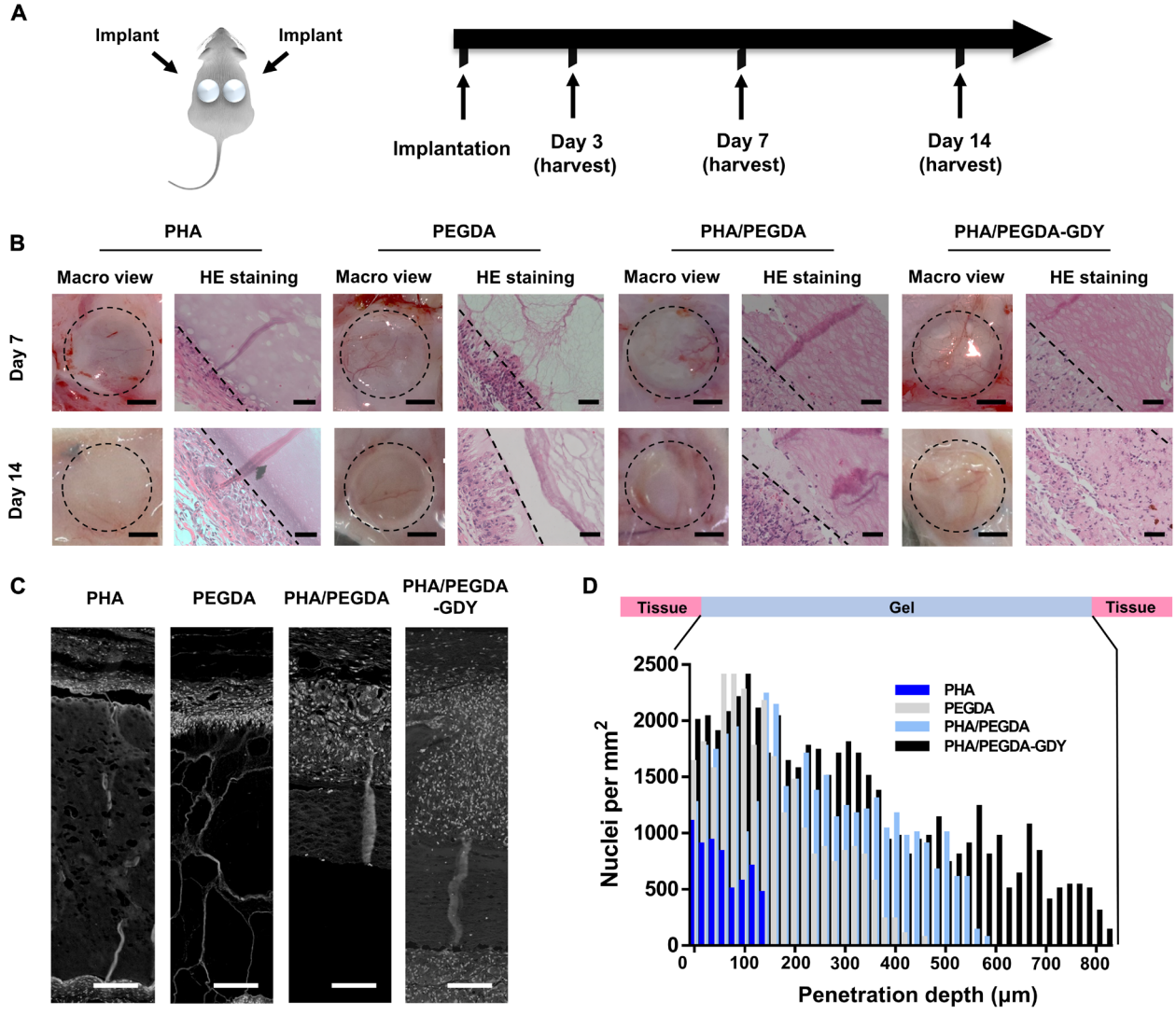

Fig. 6. In vivo implantation of cast gel disk scaffolds. (**A**) Gel scaffolds were subcutaneously implanted on the dorsa of Sprague-Dawley rats and harvested at various time points. (**B**) Macro view and hematoxylin and eosin (HE) staining images of gels at days 7 and 14 after implantation. Scale bars, 5 mm (macro view) and 50 μm (HE staining). The dashed line in HE staining: The deepest cell penetration position in scaffolds. (**C**) Processed images of HE staining showed cellular penetration of nuclei (white point) through gel scaffolds. Scale bars, 100 μm. (**D**) Mean cell density as a function of penetration depth into the gel scaffolds at 7 days after implantation.

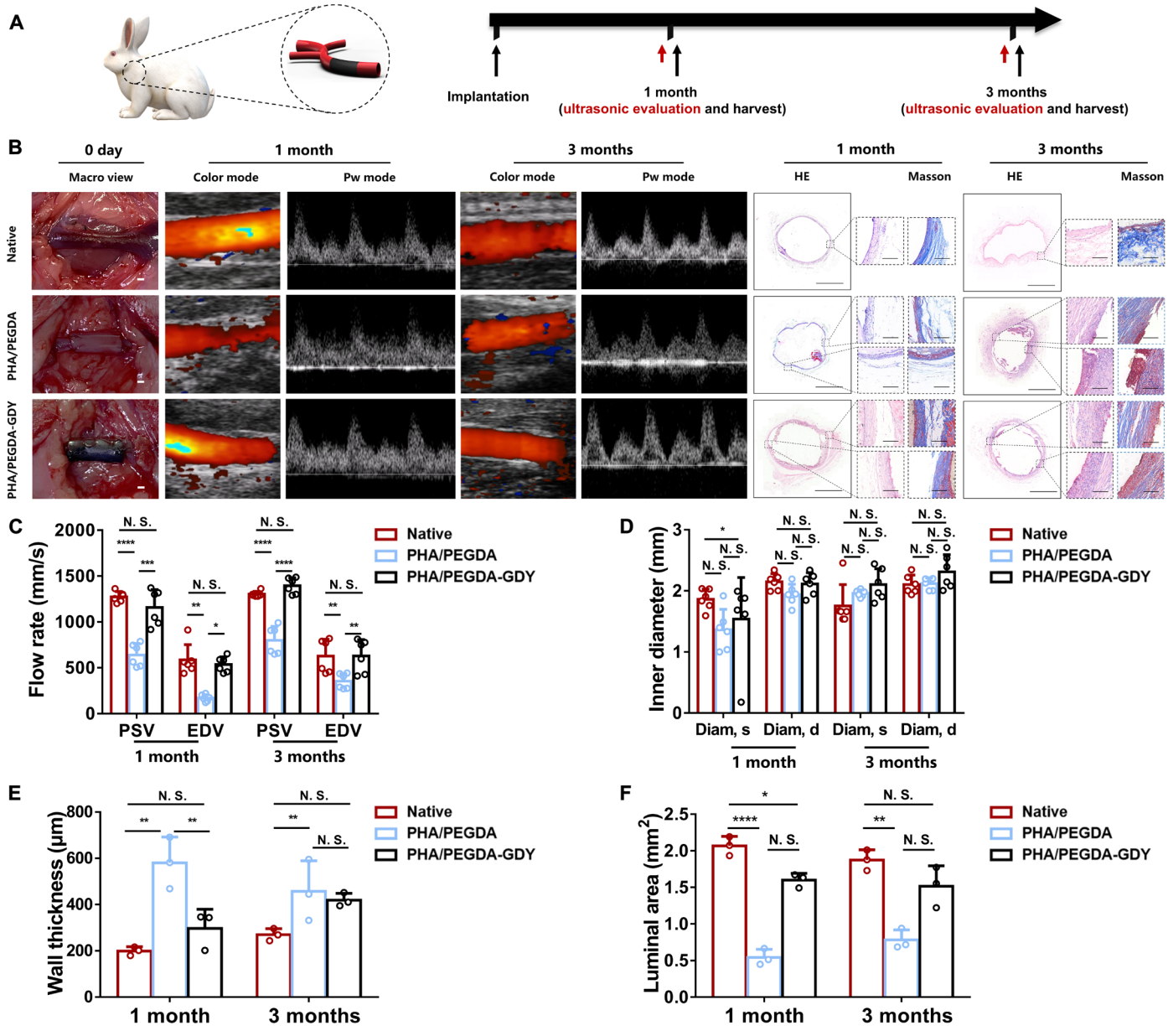

Fig. 7. In vivo implantation of gel vascular grafts. (**A**) Gel vascular grafts were implanted in rabbit model of carotid artery defect, and then ultrasound and histological evaluation of the vascular grafts were performed after 1 and 3 months of implantation. (**B**) Macroscopic views upon implantation, ultrasound images, and HE and Masson staining images after implantation of vascular grafts of gels. Scale bars, 1 mm (macro view), 1 mm (panorama), and 200 μm (magnified view). (**C**) Peak rate of blood flow and (**D**) inner diameters of vascular grafts of gels at different time points after implantation from ultrasonic evaluation ($n = 6$). (**E**) Wall thickness and (**F**) luminal area of vascular grafts explanted at different time points after implantation from histological analysis ($n = 3$). ****$P < 0.0001$, ***$P < 0.001$, **$P < 0.01$, and *$P < 0.05$ by one-way ANOVA with Tukey correction.

mechanics (fig. S20) and easy fracturing in vivo in the PHA and PEGDA groups, only the PHA/PEGDA and PHA/PEGDA-GDY groups were chosen for arterial defect repair. To evaluate the patency of the scaffolds, we monitored the blood flow in the arteries using Doppler ultrasound at time points of 1 and 3 months (Fig. 7B). The patency of the PHA/PEGDA and PHA/PEGDA-GDY groups was 66.7% (8 of 12 rabbits) and 91.7% (11 of 12 rabbits) at 1 month, respectively. Because three rabbits from each group were euthanized for histological analysis at 1 month, the overall patency at 3 months decreased to 30% (three of nine rabbits) for PHA/PEGDA group and 88.9% (eight of nine rabbits) for PHA/PEGDA-GDY group (table S1). The particular grafts failed primarily because of thrombosis. In addition, the quantitative evaluation of the flow rate in the peak systolic velocity (PSV), end diastolic velocity (EDV), and inner diameter in the systole (diam, s) and diastole (diam, d) of the PHA/PEGDA and PHA/PEGDA-GDY groups at 1 and 3 months was analyzed (Fig. 7, C and D). The PHA/PEGDA-GDY group presented faster blood flow than that of the PHA/PEGDA group for both PSV and EDV. The inner diameters of the PHA/PEGDA and PHA/PEGDA-GDY scaffolds were similar at 3 months, indicating that

the amphipathicity of the organohydrogels was beneficial for maintaining the volume of the vascular scaffolds in vivo.

The implanted grafts at 1 and 3 months after treatment were harvested for histological analysis. Cell infiltration with numerous inflammatory cells was observed in both vascular grafts, and the number of these cells decreased in 3 months. The wall thickness and luminal area of the extracted grafts were evaluated to assess the tubular structures of the organohydrogel vascular scaffolds. The PHA/PEGDA-GDY scaffolds had thinner vascular walls than the PHA/PEGDA scaffolds at 1 month, and the thickness was closer to that of the native group (Fig. 7E). This undesired thickening of the wall can lead to subsequent thrombosis and vessel occlusion. Correspondingly, the luminal areas of the PHA/PEGDA-GDY group (2.07 ± 0.11 mm^2 at 1 month and 1.87 ± 0.11 mm^2 at 3 months) were closer to those of the native group (Fig. 7F).

The responses of monocytes/macrophages to grafts during tissue regeneration are important for biomaterials (*29*). Specific makers of CD68 (a pan-marker of monocytes/macrophages), CD206 (a marker of anti-inflammatory and proregenerative macrophages, M2 macrophages), and inducible nitric oxide synthase (iNOS) (a marker of proinflammatory macrophages) were used for immunofluorescence staining (fig. S21). The grafts were infiltrated with cells marked with CD68, CD206, and iNOS at 1 month, and the number of cells significantly decreased at 3 months, indicating that M1 and M2 macrophages that migrated from circulating monocytes played an important role in tissue regeneration. In addition, it could be inferred that the PHA/PEGDA-GDY group had a much higher percentage of $CD206^+$ cells and a lower percentage of $iNOS^+$ cells than the PHA/PEGDA group, indicating that the ratio of CD206/iNOS in the PHA/PEGDA-GDY group was more proximal to that of the native group. Hence, the PHA/PEGDA-GDY vascular grafts provided a better immune microenvironment for tissue regeneration.

Remodeling of the cellular matrix and ECM remodeling in the vascular grafts was further investigated (Fig. 8A). ECM deposition is essential for mechanical support of vessels and guidance of cellular differentiation and functions (*30*). The ECM protein assembly and distribution in PHA/PEGDA-GDY scaffolds were similar to those of native vessels. Immunofluorescence staining indicated the

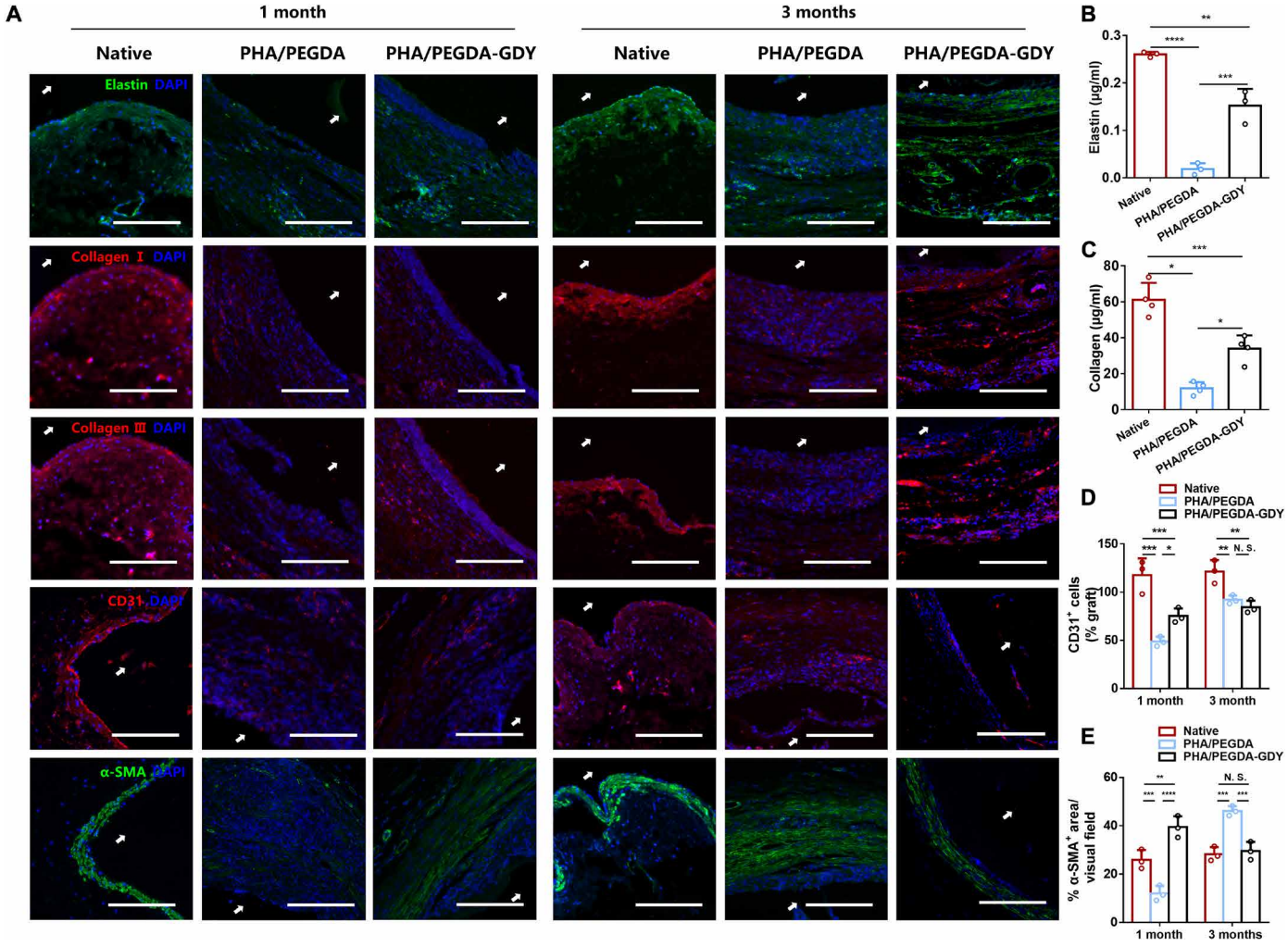

Fig. 8. Immunofluorescence staining of implanted vascular grafts after 1 and 3 months of implantation. (**A**) Immunofluorescence staining of elastin (green), collagen I (red), collagen III (red), CD31 (red), and α-SMA (green) of the grafts. White arrows indicate luminal areas. Scale bars, 200 μm. (**B**) Elastin and (**C**) collagen content in grafts explanted at the time point of 3 months ($n = 3$). Quantification analysis of $CD31^+$ cells (**D**) and percent of α-SMA^+ area (**E**) in vascular grafts ($n = 3$). ****$P < 0.0001$, ***$P < 0.001$, **$P < 0.01$, and *$P < 0.05$ by two-way ANOVA with Tukey correction.

deposition of elastin and collagens I and III across the entire scaffold. This result demonstrates that the amounts of elastin and collagen in the PHA/PEGDA-GDY scaffolds were higher than those in the PHA/PEGDA scaffolds but significantly less than those in the native vessels (Fig. 8, B and C). CD31, a typical biomarker of endothelial cells (ECs), was positively stained and gathered around the basement membrane at 3 months, indicating an endothelialization on the scaffolds. Quantitative analysis shows that the quantities of CD31-positive cells in the PHA/PEGDA-GDY scaffolds were greater than those in the PHA/PEGDA scaffolds at 1 month (Fig. 8D). The results of quantitative analysis of α–smooth muscle actin (α-SMA), indicative of SMCs, were similar to those of CD31 (Fig. 8E). However, the fluorescence intensities of α-SMA in the PHA/PEGDA scaffolds at 3 months were higher than those in the PHA/PEGDA-GDY scaffolds and even those in the native vessels, which could be related to intimal thickening. Meanwhile, the α-SMA–positive cells in PHA/PEGDA-GDY scaffolds appeared to orient in an ordered arrangement around the vascular grafts.

DISCUSSION

In this study, a novel PHA/PEGDA-GDY organohydrogel was developed as a gel vascular graft, and its potential for use in vessel defect repair was investigated. This organohydrogel vascular graft was verified with good cell biocompatibility, safety in vivo, and effectiveness in promoting tissue regeneration, which is closely associated with the good biocompatibility of PHAs. PHAs have been explored for the use in microspheres, drug vesicles, and biomedical scaffolds used in drug delivery and tissue engineering (*31*). Compared with common biopolymer polylactic acid and poly(lactic-*co*-glycolic acid), the most prominent feature of PHA is that biodegradation does not result in the fast release of lactic acid or glycolic acid, which is harmful to cells and tissues. The PHA polymer P3HB10U used in this study has unsaturated functional vinyl groups, which are important for gel amphipathicity and could be cross-linked with HS-PEG-SH (thiol-polyethylene glycol-thiol) via a click reaction. The click reaction of unsaturated functional PHA and PEGDA improved the hydrophilia of PHA and broadened its biomedical application. Moreover, because of its fast cross-linking and appropriate viscoelasticity, it could be used as an ink in digital light process 3D printing to fabricate scaffolds with complex topology.

GDY is a new 2D material with a one-atom-thick carbon allotrope composed of layers of sp- and sp^2-hybridized carbon atoms (*32*). It has been further studied in various fields because of its unique and attractive characteristic structure and physical and chemical properties. In biomedical research, GDY has shown excellent biological properties (*33*). For instance, Zhu *et al.* (*34*) studied the antibacterial activity of GDY and demonstrated that GDY could realize antibacterial mechanisms by wrapping the bacterial membrane, membrane insertion and disruption, and reactive oxygen species generation. Another research group evaluated the free radical scavenging ability and radioprotection of GDY both in vitro and in vivo. The results demonstrated that the GDY-cooperated scaffolds had good biosafety and better radioprotection activity than graphene oxide (*35*). Nevertheless, GDY has rarely been used in tissue engineering scaffolds (*33*, *36*). In this study, GDY nanoparticles were used in gels to enhance their mechanical strengths and to fabricate vascular scaffolds for implanted materials. The fatigue resistance of gels after the mixture of GDY nanoparticles has been obviously enhanced in both the tensile mechanics (>2000 cycles) and hydromechanics. The phenomenon of improved PHA/PEGDA-GDY gel modulus after 3iTT could not be verified for its self-healing or self-growing properties and may be correlated with gel fluid loss during the process. However, compared with the other groups, the mechanical enhancement of PHA/PEGDA-GDY gels indicated that PHA/PEGDA-GDY gels had hydromechanical fatigue-resistant properties. The excellent biocompatibility of GDY nanoparticles in scaffolds was pronounced both in vitro and in vivo. The pore sizes (25.43 ± 7.09 μm) and surface roughness (4.32 ± 0.73 nm) of the organohydrogels were significantly changed after the mixture of GDY nanoparticles, indicating their potential for structural modification. It was observed that those groups without GDY showed irregular twisting and bending, resulting in coarser gel surfaces. Furthermore, the porous structure is not contradictory with the smoother surface, because they reflect roughness on different scales.

Tissue engineering blood vessels, which are promising for use in vessel defect therapy, can be classified by diameter. Large-diameter vascular grafts (diameter > 6 mm) have been successfully achieved by fabricating polymeric biomaterials such as Dacron (*37*), expanded polytetrafluoroethylene (*38*), and polyurethane (*39*). Nevertheless, the replacement of SDVG has not yet been completely solved. On the one hand, because of the changes in hemodynamics (for instance, decreased blood flow velocity), thrombosis and vascular occlusion are more likely to occur than large-diameter vascular grafts (*10*). On the other hand, high failure rates were partially due to the occurrence of infection, intimal hyperplasia, and chronic inflammation (*40*). In this study, SDVGs based on PHA/PEGDA-GDY organohydrogels were fabricated to solve the aforementioned challenges. First, endothelialization is an essential process to prevent the occurrence of thrombosis and intimal hyperplasia after transplantation of vascular grafts (*41*). In the early stage, the smoother surfaces of PHA/PEGDA-GDY organohydrogel vascular grafts were found to be less likely to induce platelet aggregation and blood clotting and could provide a more appropriate microenvironment for endothelialization than the other groups. In addition, the results of cell experiments based on HUVECs and VSMCs (viability > 90%) illustrated that PHA/PEGDA-GDY organohydrogels were suitable biomaterials that facilitate the proliferation of ECs and SMCs. With cell infiltration in gels after implantation, there were more $CD31^+$ cells gathering in PHA/PEGDA-GDY organohydrogel vascular grafts than in the other grafts. Second, vascular grafts should not only mimic the tensile moduli of normal vessels but also have fatigue resistance, self-healing abilities, and modulus stability. In addition, the tensile moduli and rupture strain of the PHA/PEGDA-GDY organohydrogels were 167.64 ± 39.93 and 117.70 ± 9.61 kPa, which was slightly lower than those of normal vessels. Nevertheless, note that, considering biocompatibility and biodegradation, most hydrogels applied as biomedical materials may not be able to have extremely high mechanical strengths. Moreover, the limited hydrophilia of organohydrogels contributed to maintaining their mechanical stability after implantation. This unique characteristic of organohydrogels demonstrates their potential for further applications, as most hydrogels become soft and fragile after immersion in body fluids. Last, the surface structure that was in direct contact with the blood significantly influenced the subsequent biodegradation and tissue growth. GDY nanoparticle–modified organohydrogels presented porous structures with pore sizes of approximately 30 μm, which has already been verified to be beneficial for cell infiltration and

tissue regeneration. The investigation of biocompatibility in vivo indicated that cells could reach a penetration depth of 800 μm after 14 days of implantation.

However, some existing limitations remain in this research. First, it cannot be denied that additional endeavors are required to improve the mechanics of PHA/PEGDA-GDY gels (including ultimate tensile and rupture strains) to achieve clinical vascular graft standards. Second, it is essential to evaluate various sizes of gel SDVG to broaden their applications. Last but not least, implantation in large rodents, such as rabbits, was not sufficient to confirm the possibility for clinic use, and thus, it must undergo a preclinical study of PHA/PEGDA-GDY organohydrogels as vascular grafts in large animal models, such as pigs and cynomolgus monkeys.

In summary, we designed and successfully fabricated PHA/PEGDA-GDY organohydrogels with appropriate amphipathicity, fatigue resistance, and good biocompatibility both in vitro and in vivo. Moreover, when applied as vascular grafts, PHA/PEGDA-GDY showed excellent cell infiltration, few undesirable immune responses, and good tissue regeneration for cellular components (ECs and SMCs) and ECM (collagen and elastin). Moreover, this research illustrated the possibility of organohydrogels based on PHA and PEGDA as one of promising biomaterials and vital roles of GDY nanoparticles in mechanical strengthening. The excellent properties of PHA/PEGDA-GDY organohydrogels make them suitable for further application in biomaterials and regenerative medicine.

MATERIALS AND METHODS

Synthesis of P3HB10U

P3HB10U was produced using an engineered strain of *P. entomophila* (LAC32) based on a cultivation procedure modified from a previously reported method (*21*). Briefly, *P. entomophila* LAC32 was inoculated in a 100-ml Erlenmeyer flask containing 20 μl of kanamycin and 20 m of lysogeny broth (LB) medium containing tryptone (10 g/liter), yeast extract (5 g/liter), and NaCl (10 g/liter). Subsequently, 5% (v/v) seed cultures and 0.1% (v/v) kanamycin were inoculated into a four-yeast LB medium containing tryptone (12 g/liter) and yeast extract (24 g/liter), which was cocultured with different ratios of glucose and 10-undecenoic acid to control the alkene content. After cultivation for 48 hours at 30°C in a rotary shaker (200 rpm), the cells were collected by centrifugation at 8000 rpm for 20 min at room temperature, and the supernatant was discarded. The collected strains were washed with absolute ethanol to remove residual carbon sources, collected again by centrifugation under the same conditions, and washed with deionized water. PHA was dried by lyophilization and purified via Soxhlet extraction followed by ethanol precipitation. Soxhlet extractions were performed in 120 ml of chloroform for 4 hours, and then the solution was evaporated under ventilated conditions for no less than 5 hours. The resulting film was dissolved in a minimal amount of chloroform and precipitated using a 10-fold volume of ethanol. The final white PHA powder was obtained after the freeze-drying process, characterized by NMR (AVANCE AV 400 MHz, Bruker, Swiss), and stored at room temperature protected from light until organohydrogel fabrication began.

Preparation of PHA/PEGDA-GDY organohydrogels

To optimize the reaction condition of PHA organogel, P3HB10U with 15 and 45% alkene was reacted with HS-PEG-SH (Aladdin, China) of 1000 Da (#T164378), 2000 Da (#T164381), and 5000 Da (#T164386) at equivalent ratios of 1:0.25 and 1:0.5. The degree of cross-linking at different time points was recorded on the basis of whether the solution samples ($n = 4$) became gels or not. The degree of adhesion was evaluated according to the following standard: 0% solution, 25% floccule, 50% gel-like substances, 75% gel but easily torn, and 100% gel with intact structure.

Briefly, the PHA/PEGDA solution was prepared by dissolving 0.100 g of P3HB10U with 45% vinyl group, 0.160 g of HS-PEG-SH (2000 Da), and 0.260 g of PEGDA (#729094, Sigma-Aldrich, USA) in 2.7 ml of anhydrous tetrahydrofuran (THF; #1.15088.026, Guangdong Guanghua Sci-Tech, China) in a glass bottle at 40°C under agitation for at least 30 min. In addition, 10 mg of GDY nanoparticles (#102499, XFNano, China) were dispersed in 1 ml of THF containing 5 mg of SDS (#S118591, Aladdin, China) via sonication dispersion (200 to 300 W, 40 Hz). Then, 0.3 ml of GDY solution was added to the PHA/PEGDA solution and dispersed for another 10 min. After complete blending, 2 mg of photoinitiator benzoin dimethyl ether (#M11768, China) and 5 mg of Irgacure 2959 (#410896, Sigma-Aldrich, USA) were added to the mixture solution. The solutions were poured into the molds and exposed to ultraviolet irradiation (6.9 mW/cm^2, 360 to 480 nm). The gelation time was evaluated using the vial tilting method. After cross-linking, the PHA/PEGDA-GDY organohydrogels were immersed in chloroform for 2 hours to remove unreacted substances and residual THF. Subsequently, the organohydrogels were immersed in 75% ethyl alcohol for 48 hours to dissolve the chloroform, and the alcohol was changed every 24 hours. Last, the organohydrogels were stored in 75% ethyl alcohol or deionized water.

Characterization and morphology of PHA/PEGDA-GDY organohydrogels

To test the amphipathy of the gels, the gels were cut into flat sheets with diameters of 8 mm and thicknesses of 5 mm. After immersion in deionized water for 24 hours or in chloroform for 2 hours, the weight and diameter were measured, and the diameter and swelling ratios were calculated. The CA and SFE were also determined. All CAs were measured using a CA meter (OCA-40, DataPhysics, Germany) at ambient temperature. The droplet volume was precisely controlled at 2 μl. In addition, the organic fluid was diiodomethane. Last, to study the variations in the surface states of the different groups further, the SFE, which demonstrated the wettability characteristics, was calculated using the Owens-Wendt method (*42*)

$$\gamma_l(1 + \cos\theta_\gamma)/2 = (\gamma_s^d \gamma_l^d)^{1/2} + (\gamma_s^p \gamma_l^p)^{1/2}$$
$$\gamma_s = \gamma_s^d + \gamma_s^p$$
$$\gamma_l = \gamma_l^d + \gamma_l^p$$

where θ_γ is the CA between the solid and liquid phases and s and l are the SFEs of the solid and liquid phases, respectively. γ_s^d and γ_s^p refer to the dispersion force component and polar force component of the SFE of the solid (SFE*d* and SFE*p*), respectively, and γ_l^d and γ_l^p represent the dispersion and polar force components of the SFE of the liquid (SFE*d* and SFE*p*), respectively. Table S2 presents the related data. The experiments above have been technically repeated at least three times.

FTIR spectroscopy (VERTEX 70, Bruker, Germany) was used to detect the chemical bond changes in the gels. The FTIR measurements were conducted in the frequency range of 4000 to 500 cm^{-1}.

The tests were performed using a diode laser with a wavelength of 532 nm at ambient temperature. Cryo-EM imaging was performed on a cold field-emission scanning electron microscope (S-4800, HITACHI, Japan) fitted with a low-temperature sample carrier (Quorum PP3000T) to observe the hydrogel morphology. The samples were placed in a cryo-specimen holder, fixed in cold nitrogen (−120°C), and then rapidly transferred to the cryo-stage in the frozen state. The sample temperature was raised by heating the holder to 90°C for 30 min to increase the contrast and sublimate free water in the solid-state lakes, followed by a temperature decrease to −180°C to stabilize the sample. The samples were transferred to a microscope to observe the normal surface of the hydrogel. A scanning electron microscope (SU-70, HITACHI, Japan) set at an accelerating voltage of 10 kV was used to observe the microstructures of the gels after lyophilization. The scaffold surfaces were sprayed with platinum using a sputter coater before measurement. AFM was performed to measure the gel topography. The samples were cross-linked on a mica plate and tested on a Bruker MultiMode 8 scanning probe microscope (Veeco, America) in tapping mode.

Mechanical properties of PHA/PEGDA-GDY gels

Tensile tests

The gels were cut into uniform strips, and the dimensions (30 mm by 10 mm by 2 mm) of the gel samples were measured using a digital caliper. An all-electric dynamic test instrument (Instron, British) was used to measure the mechanical properties of the scaffolds. The samples were tightly fixed to two clamps and stretched at a constant rate of 10 mm/min. According to the results, the tensile properties of the samples, including the tensile modulus (the tangent slope of the stress-strain curve), ultimate strength (stress at failure), and rupture strain or extensibility (strain level at failure) were calculated. Cyclic tensile tests were performed using a cross-speed of 10 mm/min and a 50% strain level for 2000 cycles. The energy loss before and after the cycles was calculated on the basis of the area between the loading and unloading curves. Suture retention experiments were performed by stretching the 5-0 suture pierced through at 5 mm from the gel edges at a speed of 10 mm/min. The ultimate suture retention strength was recorded at failure incidence. All of the above data and plots were obtained using OriginPro software (OriginLab, USA).

Rheological tests

The gels were cut into uniform disks with a diameter of 10 mm and a thickness of 1 mm. The amplitude sweep (AS), frequency sweep (FS), and 3iTT were performed using a modular compact rheometer (MCR 102, Anton Paar, Germany). The gels were tested by running the shear strain from 0.01 to 1000% at a constant frequency of 1 Hz to analyze the AS and tested by running the frequency from 0.1 to 10 Hz at a constant shear strain of 100% to analyze the FS. The effects of the shear rate on the specimen deformation were investigated using the 3iTT method at a temperature of 25°C. In the middle interval, the samples were deformed at a constant shear strain of γ_{max} = 100%. In the initial and final intervals, the gels were measured at a constant deformation amplitude γ_{min} = 0.5% to establish the properties before and after the rotational deformation process. The experiments above have been technically repeated at least three times.

In vitro cell biocompatibility of PHA/PEGDA-GDY organohydrogels

The cell viability (the percent of live cells in all cells of gels) within the gels was evaluated using HUVECs [#PCS-100-010, American Type Culture Collection (ATCC), USA] and VSMCs (#CRL-1999, ATCC, USA). The HUVECs were cultured in RPMI 1640 medium (#C11875500BT, Gibco, USA) supplemented with 10% fetal bovine serum (FBS; #10099141, Gibco, USA) and 1% penicillin/streptomycin (P/S; #15070063, Gibco, USA) at 37°C under 5% CO_2, whereas the VSMCs were cultured in F12K medium (#21127030, Gibco, USA) supplemented with 10% FBS and 1% P/S. The medium was exchanged every 2 days, and the cells were passaged before reaching 80% confluence. The CCK8 assay was performed as follows. The gels were sterilized in 75% ethyl alcohol, cut into slides with a diameter of 2 mm, and placed in 24-well plates. Then, the HUVECs/VSMCs were prepared at a density of 1.0×10^4 cells/ml, and 100 μl of the cell suspension was added to each sample. At time points of 1 to 6 days, a mixture of 100 μl of complete medium and 10 μl of CCK-8 was added to each well and incubated for 4 hours at 37°C. The supernatant was then transferred into each well of a 96-well plate, and the absorbance at 450 nm was measured using an absorbance microplate reader (ELx800, BioTek, USA). FDA/PI staining of samples was performed as previously reported (*43*). In addition, CD31 immunofluorescence staining was conducted using rabbit anti-CD31 antibody (#ab28364, Abcam, USA) as the primary antibody and goat anti-rabbit immunoglobulin G (IgG) H&L (Alexa Fluor 594 conjugate) (#ab150088, Abcam, USA) as the secondary antibody, whereas mouse α-SMA (#A5228, Sigma-Aldrich, USA) immunofluorescence staining was performed using the primary antibody and goat anti-mouse IgG H&L (Alexa Fluor 488 conjugate) (#ab150117, Abcam, USA) as the secondary antibody. In addition, 4′,6-diamidino-2-phenylindole (DAPI) staining was conducted (#D9542, Sigma-Aldrich, USA). The HUVECs were implanted into the gels with a density of 1×10^5 per ml and cultured under the conditions described above. The cell-seeded samples were washed with phosphate-buffered saline after 24 and 48 hours and fixed with 4% paraformaldehyde. Cell staining was performed using fluorescein isothiocyanate–labeled phalloidin (#P5282, Sigma-Aldrich, USA). All samples were observed using a laser scanning confocal microscope (LSM800, Leica, Germany). The experiments above have been biologically repeated at least twice.

Millimeter-scale PHA/PEGDA-GDY gel tubes: Fabrication, perfusion, and vascular characterization

The gel tubes were designed to approximate the scale of SDVGs (2 to 6 mm in diameter) using the molding methods. The gel tubes were fabricated with inner diameters of 2 mm, outer diameters of 3 mm, and lengths of 10 mm through the corresponding quartz glass tube. After implementing the washing operation mentioned above and sterilization, the gel tubes were prepared for further studies.

For the perfusion experiments, the gel tube constructs were carefully connected to a perfusion tube, launched by a peristaltic pump (BT100-2J, Longer, China). The perfusion within the tube lumen and diffusion through the tube wall were visualized using a 5% glucose solution mixture with 0.1% rhodamine (#R817327, Macklin, China). Fluorescent time-lapse videos and images were obtained using a fluorescent stereomicroscope (Axio Zoom.V16, Carl Zeiss, Germany).

Cell implantation in the gel tubes was performed as follows. HUVECs and VSMCs were collected before reaching an 80% confluence and prepared as a cell suspension at a concentration of 1×10^6 per ml. Then, 1 ml of suspension was perfused into the gel tubes, and the tubes were kept in a constant and slow rotation state

for 2 hours and then moved into the bioreactor, as depicted in fig. S16. After culturing for 7 and 14 days in the bioreactor, the tube was fixed in 4% paraformaldehyde and cut into slices at a thickness of 10 μm using a rotary microtome (RM2255, Leica, Germany). The samples were stained with DAPI and CD31/α-SMA and observed under a laser scanning confocal microscope, as described above.

In vivo biocompatible assessment of PHA/PEGDA-GDY organohydrogels

Gel disks with diameters of 10 mm and heights of 5 mm were cast and washed to remove excess solvents. After sterilization, the gel disks were implanted on the dorsa of Sprague-Dawley male rats (6 to 8 weeks old). All experimental and animal care procedures in this study were performed at the Guangzhou Institute of Biomedicine and Health, Chinese Academy of Sciences in accordance with the Institutional Animal Care and Use Committee (no. N2019066). The entire operation process was conducted by the same surgeon on a laminar clean bench under anesthesia (2% isoflurane inhalation).

After hair shaving and skin disinfection, the gel disks were implanted subcutaneously for 3, 7, and 14 days (n = 8 rats per group) to evaluate the effects of the gels on cellular infiltration and tissue regeneration. For harvesting, the gel disks were cleaned of connective adipose tissue and fixed in 4% paraformaldehyde overnight before embedding in paraffin. The paraffin was sectioned along the midlines of the disks (5 μm), the sections were stained with HE, and bright-field images of the stained sections were acquired using a scanning microscope (VMV1 VMDPCS, Motic, China). To evaluate the cellular penetration into the implanted gel disks further, HE staining images were processed in black and white mode, and the nuclei appeared as white points. The experiments above have been biologically repeated at least twice.

In vivo implantation evaluation on rabbit carotid artery model

Vascular scaffolds were fabricated with inner diameters of 2 mm, outer diameters of 3 mm, and lengths of 10 mm and were implanted into the rabbit carotid artery model to assess the repair effects of scaffolds in vivo further. All experimental and animal care procedures were performed in accordance with the principles mentioned above. Twenty-four male New Zealand white rabbits (2.0 to 2.3 kg) were randomly divided into two groups of PHA/PEGDA scaffolds and PHA/PEGDA-GDY scaffolds. The rabbits were injected with 5 ml of 2.5% sterile pentobarbital sodium solution from the auricular vein for general anesthesia. After the rabbits were completely unconscious, the hair around the neck was shaved and applied with depilatory cream, then the rabbits were gently fixed on a minor operation table, and the neck region was disinfected. We incised the epidermal layer, corium layer, and muscles to expose fully and separate the left internal carotid artery. A section of the artery (approximately 20 mm) was transected between the clamp, and a vascular graft was implanted and sutured to the defect of the rabbit carotid artery after the anastomotic site was rinsed with heparin sodium saline and diluted scopolamine solution. Normal blood flow was observed after removing the clamps, and after careful hemostasis, the wounds were closed with 3-0 nonabsorbable suture (Ethicon, USA). Aspirin was administered daily postoperatively as an anticoagulant for at least 7 days. All procedures were conducted by the same group of surgeons using the same procedure.

Doppler ultrasound assessment was performed on rabbits implanted with gel vascular grafts at 1 and 3 months using an ultrasound imaging system for small animals (Vevo 2100, Fuji, Canada). Before ultrasonic evaluation, the rabbits were anesthetized as described and had hair around the neck cleaned. The color mode and pulse wave mode were used to evaluate the patency, diastole and systole diameters, and flow velocities, such as the end EDV and PSV.

For histological staining and immunofluorescence staining, the extract vascular scaffolds were fixed, embedded in paraffin, and sectioned as described above. Table S3 lists the antibodies used for immunofluorescence. The collagen content of explanted grafts and native vessels was measured using the Total Collagen Assay Kit (#GMS50326.2, GenMed Scientifics Inc., America), and the elastin content of explanted scaffolds was measured using the Elastin Assay Kit (#GMS50691.2, GenMed Scientifics Inc., America). Three different samples (n = 3) were analyzed for each group. The experiments above have been technically repeated at least three times.

Statistical analysis

All data are shown as the means ± SD. Each assay had at least three replicates and was repeated three times independently. One-way analysis of variance (ANOVA) or two-way ANOVA followed by Tukey, Sidak, or Bonferroni correction or the two-tailed Student's t test was performed to analyze the statistical significance. Statistical significance was set at $P < 0.05$.

SUPPLEMENTARY MATERIALS

Supplementary material for this article is available at https://science.org/doi/10.1126/sciadv.abn5360

View/request a protocol for this paper from *Bio-protocol*.

REFERENCES AND NOTES

1. N. Annabi, A. Tamayol, J. A. Uquillas, M. Akbari, L. E. Bertassoni, C. Cha, G. Camci-Unal, M. R. Dokmeci, N. A. Peppas, A. Khademhosseini, 25th anniversary article: Rational design and applications of hydrogels in regenerative medicine. *Adv. Mater.* **26**, 85–124 (2014).
2. T. E. Brown, K. S. Anseth, Spatiotemporal hydrogel biomaterials for regenerative medicine. *Chem. Soc. Rev.* **46**, 6532–6552 (2017).
3. J. Fang, J. Koh, Q. Fang, H. Qiu, M. M. Archang, M. M. Hasani-Sadrabadi, H. Miwa, X. Zhong, R. Sievers, D.-W. Gao, R. Lee, D. D. Carlo, S. Li, Injectable drug-releasing microporous annealed particle scaffolds for treating myocardial infarction. *Adv. Funct. Mater.* **30**, 2004307 (2020).
4. W. Zhu, C. Chu, S. Kuddannaya, Y. Yuan, P. Walczak, A. Singh, X. Song, J. W. M. Bulte, *In vivo* imaging of composite hydrogel scaffold degradation using CEST MRI and two-color NIR imaging. *Adv. Funct. Mater.* **29**, 1903753 (2019).
5. Z. Chen, F. Liu, Y. Chen, J. Liu, X. Wang, A. T. Chen, G. Deng, H. Zhang, J. Liu, Z. Hong, J. Zhou, Targeted delivery of CRISPR/Cas9-mediated cancer gene therapy *via* liposome-templated hydrogel nanoparticles. *Adv. Funct. Mater.* **27**, 1703036 (2017).
6. N. Alexandre, E. Costa, S. Coimbra, A. Silva, A. Lopes, M. Rodrigues, M. Santos, A. C. Maurício, J. D. Santos, A. L. Luís, *In vitro* and *in vivo* evaluation of blood coagulation activation of polyvinyl alcohol hydrogel plus dextran-based vascular grafts. *J. Biomed. Mater. Res. A* **103**, 1366–1379 (2015).
7. R. Xie, W. Zheng, L. Guan, Y. Ai, Q. Liang, Engineering of hydrogel materials with perfusable microchannels for building vascularized tissues. *Small* **16**, e1902838 (2020).
8. Y. C. Chen, R. Z. Lin, H. Qi, Y. Yang, H. Bae, J. M. Melero-Martin, A. Khademhosseini, Functional human vascular network generated in photocrosslinkable gelatin methacrylate hydrogels. *Adv. Funct. Mater.* **22**, 2027–2039 (2012).
9. H. Kamata, Y. Akagi, Y. Kayasuga-Kariya, U.-I. Chung, T. Sakai, "Nonswellable" hydrogel without mechanical hysteresis. *Science* **343**, 873–875 (2014).
10. A. Goins, A. R. Webb, J. B. Allen, Multi-layer approaches to scaffold-based small diameter vessel engineering: A review. *Mater. Sci. Eng. C* **97**, 896–912 (2019).
11. S. Fleischer, D. N. Tavakol, G. Vunjak-Novakovic, From arteries to capillaries: Approaches to engineering human vasculature. *Adv. Funct. Mater.* **30**, 1910811 (2020).
12. C. Shen, Y. Li, Y. Wang, Q. Meng, Non-swelling hydrogel-based microfluidic chips. *Lab Chip* **19**, 3962–3973 (2019).

13. N. Annabi, S. R. Shin, A. Tamayol, M. Miscuglio, M. A. Bakooshli, A. Assmann, P. Mostafalu, J.-Y. Sun, S. Mithieux, L. Cheung, X. S. Tang, A. S. Weiss, A. Khademhosseini, Highly elastic and conductive human-based protein hybrid hydrogels. *Adv. Mater.* **28**, 40–49 (2016).
14. D. G. Seifu, A. Purnama, K. Mequanint, D. Mantovani, Small-diameter vascular tissue engineering. *Nat. Rev. Cardiol.* **10**, 410–421 (2013).
15. Z. Zhang, J. Hao, Bioinspired organohydrogels with heterostructures: Fabrications, performances, and applications. *Adv. Colloid Interface Sci.* **292**, 102408 (2021).
16. Z. Zhao, K. Zhang, Y. Liu, J. Zhou, M. Liu, Highly stretchable, shape memory organohydrogels using phase-transition microinclusions. *Adv. Mater.* **29**, 1701695 (2017).
17. H. Gao, Z. Zhao, Y. Cai, J. Zhou, W. Hua, L. Chen, L. Wang, J. Zhang, D. Han, M. Liu, L. Jiang, Adaptive and freeze-tolerant heteronetwork organohydrogels with enhanced mechanical stability over a wide temperature range. *Nat. Commun.* **8**, 15911 (2017).
18. S. Zhuo, Z. Zhao, Z. Xie, Y. Hao, Y. Xu, T. Zhao, H. Li, E. M. Knubben, L. Wen, L. Jiang, M. Liu, Complex multiphase organohydrogels with programmable mechanics toward adaptive soft-matter machines. *Sci. Adv.* **6**, eaax1464 (2020).
19. Y. Liu, L. Wang, H. Lu, Z. Huang, Gelator-enhanced organohydrogels with switchable mechanics and high-strain shape-memory capacity. *Langmuir* **37**, 6711–6721 (2021).
20. Z. Zhao, C. Li, Z. Dong, Y. Yang, L. Zhang, S. Zhuo, X. Zhou, Y. Xu, L. Jiang, M. Liu, Adaptive superamphiphilic organohydrogels with reconfigurable surface topography for programming unidirectional liquid transport. *Adv. Funct. Mater.* **29**, 1807858 (2019).
21. M. Li, Y. Ma, X. Zhang, L. Zhang, X. Chen, J.-W. Ye, G.-Q. Chen, Tailor-made polyhydroxyalkanoates by reconstructing pseudomonas entomophila. *Adv. Mater.* **33**, e2102766 (2021).
22. X. Zhang, Y. Lin, Q. Wu, Y. Wang, G.-Q. Chen, Synthetic biology and genome-editing tools for improving PHA metabolic engineering. *Trends Biotechnol.* **38**, 689–700 (2020).
23. M. Li, X. Chen, X. Che, H. Zhang, L.-P. Wu, H. Du, G.-Q. Chen, Engineering pseudomonas entomophila for synthesis of copolymers with defined fractions of 3-hydroxybutyrate and medium-chain-length 3-hydroxyalkanoates. *Metab. Eng.* **52**, 253–262 (2019).
24. X. Zhang, Z. Li, X. Che, L. Yu, W. Jia, R. Shen, J. Chen, Y. Ma, G.-Q. Chen, Synthesis and characterization of polyhydroxyalkanoate organo/hydrogels. *Biomacromolecules* **20**, 3303–3312 (2019).
25. S. R. Shin, H. Bae, J. M. Cha, J. Y. Mun, Y.-C. Chen, H. Tekin, H. Shin, S. Farshchi, M. R. Dokmeci, S. Tang, A. Khademhosseini, Carbon nanotube reinforced hybrid microgels as scaffold materials for cell encapsulation. *ACS Nano* **6**, 362–372 (2012).
26. T. L. Sun, T. Kurokawa, S. Kuroda, A. B. Ihsan, T. Akasaki, K. Sato, M. A. Haque, T. Nakajima, J. P. Gong, Physical hydrogels composed of polyampholytes demonstrate high toughness and viscoelasticity. *Nat. Mater.* **12**, 932–937 (2013).
27. Y. Yue, T. Kurokawa, M. A. Haque, T. Nakajima, T. Nonoyama, X. Li, I. Kajiwara, J. P. Gong, Mechano-actuated ultrafast full-colour switching in layered photonic hydrogels. *Nat. Commun.* **5**, 4659 (2014).
28. L. R. Madden, D. J. Mortisen, E. M. Sussman, S. K. Dupras, J. A. Fugate, J. L. Cuy, K. D. Hauch, M. A. Laflamme, C. E. Murry, B. D. Ratner, Proangiogenic scaffolds as functional templates for cardiac tissue engineering. *Proc. Natl. Acad. Sci. U.S.A.* **107**, 15211–15216 (2010).
29. J. Fu, M. Wang, I. De Vlaminck, Y. Wang, Thick PCL fibers improving host remodeling of PGS-PCL composite grafts implanted in rat common carotid arteries. *Small* **16**, e2004133 (2020).
30. C. Camillo, N. Facchinello, G. Villari, G. Mana, N. Gioelli, C. Sandri, M. Astone, D. Tortarolo, F. Clapero, D. Gays, R. E. Oberkersch, M. Arese, L. Tamagnone, D. Valdembri, M. M. Santoro, G. Serini, LPHN2 inhibits vascular permeability by differential control of endothelial cell adhesion. *J. Cell Biol.* **220**, e202006033 (2021).
31. D. X. Wei, J. W. Dao, G. Q. Chen, Highly open porous polyhydroxyalkanoate microspheres as injectable scaffolds for tissue regeneration. *Adv. Mater.* **30**, e1802273 (2018).
32. X. Gao, Y. Zhu, D. Yi, J. Zhou, S. Zhang, C. Yin, F. Ding, S. Zhang, X. Yi, J. Wang, L. Tong, Y. Han, Z. Liu, J. Zhang, Ultrathin graphdiyne film on graphene through solution-phase van der Waals epitaxy. *Sci. Adv.* **4**, eaat6378 (2018).
33. J. Liu, C. Chen, Y. Zhao, Progress and prospects of graphdiyne-based materials in biomedical applications. *Adv. Mater.* **31**, e1804386 (2019).
34. Z. Zhu, Q. Bai, S. Li, S. Li, M. Liu, F. Du, N. Sui, W. W. Yu, Antibacterial activity of graphdiyne and graphdiyne oxide. *Small* **16**, e2001440 (2020).
35. J. Xie, C. Wang, N. Wang, S. Zhu, L. Mei, X. Zhang, Y. Yong, L. Li, C. Chen, C. Huang, Z. Gu, Y. Li, Y. Zhao, Graphdiyne nanoradioprotector with efficient free radical scavenging ability for mitigating radiation-induced gastrointestinal tract damage. *Biomaterials* **244**, 119940 (2020).
36. R. Wang, M. Shi, F. Xu, Y. Qiu, P. Zhang, K. Shen, Q. Zhao, J. Yu, Y. Zhang, Graphdiyne-modified TiO_2 nanofibers with osteoinductive and enhanced photocatalytic antibacterial activities to prevent implant infection. *Nat. Commun.* **11**, 4465 (2020).
37. H. Ma, J. Hu, P. X. Ma, Polymer scaffolds for small-diameter vascular tissue engineering. *Adv. Funct. Mater.* **20**, 2833–2841 (2010).
38. B. Jiang, L. Perrin, D. Kats, T. Meade, G. Ameer, Enabling non-invasive assessment of an engineered endothelium on ePTFE vascular grafts without increasing oxidative stress. *Biomaterials* **69**, 110–120 (2015).
39. P. Davoudi, S. Assadpour, M. A. Derakhshan, J. Ai, A. Solouk, H. Ghanbari, Biomimetic modification of polyurethane-based nanofibrous vascular grafts: A promising approach towards stable endothelial lining. *Mater. Sci. Eng. C Mater. Biol. Appl.* **80**, 213–221 (2017).
40. L. P. Frazão, A. M. Fernandes, C. Oliveira, A. Martins, T. H. Silva, J. V. De Castro, C. Nogueira-Silva, N. M. Neves, New vascular graft using the decellularized human chorion membrane. *ACS Biomater. Sci. Eng.* **7**, 3423–3433 (2021).
41. Z. Zeng, C. Hu, Q. Liang, L. Tang, D. Cheng, C. Ruan, Coaxial-printed small-diameter polyelectrolyte-based tubes with an electrostatic self-assembly of heparin and YIGSR peptide for antithrombogenicity and endothelialization. *Bioact. Mater.* **6**, 1628–1638 (2020).
42. D. K. Owens, R. C. Wendt, Estimation of the surface free energy of polymers. *J. Appl. Polym. Sci.* **13**, 1741–1747 (1969).
43. J. Hou, L. Chen, M. Zhou, J. Li, J. Liu, H. Fang, Y. Zeng, J. Sun, Z. Wang, Multi-layered polyamide/collagen scaffolds with topical sustained release of N-acetylcysteine for promoting wound healing. *Int. J. Nanomedicine* **15**, 1349–1361 (2020).

Acknowledgments: We acknowledge the technical support of L. Zhong for AFM measurements. **Funding:** L.-P.W. acknowledges financial support from the National Key R&D Program of China (no. 2019YFA0110500), International Science and Technology Cooperation Program of Guangdong Province (no.2019A050510028), and Guangdong Pearl River Talents Program (no. 2017GC010411). J.S. acknowledges financial support from the National Natural Science Foundation of China (nos. 82020108020 and 81873941). G.-Q.C. acknowledges financial support from the Ministry of Science and Technology of China (no. 2018YFA0900200), National Natural Science Foundation of China (nos. 21761132013 and 31870859), Tsinghua University-INDITEX Sustainable Development Fund (no. TISD201907), and Center of Life Sciences of Tsinghua-Peking University. G.-Q.C. also acknowledges financial support from the National Natural Science Foundation of China (nos. 31961133017, 31961133018, and 31961133019). These grants are part of MIX-UP, a joint NSFC and European Union Horizon 2020 collaboration. In Europe, MIX-UP has received funding from the European Union's Horizon 2020 research and innovation programme under grant agreement no. 870294.
Author contributions: L.-P.W., J.S., and G.-Q.C. conceived the idea. J.H., X.Z., and Z.W. prepared the materials, performed the physicochemical characterization, and analyzed the data. J.H., Y.W., J.J., and Z.W. carried out the cytological experiment and analyzed the data. J.H., J.J., Z.W., and J.S. contributed to animal experiments, tissue processing, immunostaining, and data analysis. G.-Q.C., L.-P.W., and J.S. provided financial support. J.H. prepared the manuscript with inputs from all authors. L.-P.W., J.S., and G.-Q.C. supervised the project and revised the manuscript. All authors commented on the manuscript and its revisions. **Competing interests:** The authors declare that they have no competing interests. **Data and materials availability:** All data needed to evaluate the conclusions in the paper are present in the paper and/or the Supplementary Materials.

Submitted 6 December 2021
Accepted 15 June 2022
Published 29 July 2022
10.1126/sciadv.abn5360